Acta Cryst. (1977). A33, 758–767

Problems in the Numerical Calculation of the Contrast of Defects in X-ray Traverse Topographs

BY Y. EPELBOIN

Laboratoire de Minéralogie–Cristallographie, associé au CNRS, Université P. & M. Curie, 4 place Jussieu, 75230 Paris CEDEX 05, France

(*Received* 24 *January* 1977; *accepted* 23 *March* 1977)

The simulation of section topographs of distorted crystals may be performed with good accuracy; it is now possible to use it as a tool to determine the quantitative parameters of various defects. The simulation of traverse topographs is a more complicated problem: it needs a tremendous amount of computation time, but the main difficulty arises from the numerical method itself. Reasons and a demonstration, with simulations of the contrast of a dislocation, are given why the only way to compute the traverse topograph is by the addition of the intensities due to an incident spherical wave. Nevertheless, the accuracy of the result remains poor.

Introduction

The calculation of the contrast of a dislocation was first performed by Taupin (1964, 1967) in the case of an incident plane wave with an infinite width. Then, Authier, Malgrange & Tournarie (1968) calculated the repartition of the intensity of the X-rays when the crystal is curved by a thermal gradient. Authier & Balibar (1967) simulated, for the first time, a section topograph in the case of an isotropic crystal containing a dislocation. Since then, several authors have developed routines to simulate section topographs: Chukovskii (1974), Epelboin (1974), Takagi, Ishida, Komaki & Saito (1974), in the Laue case and Bedynska (1973) in the Bragg case. Ishida, Miyamoto & Kohra (1976) have simulated the image of a dislocation in the case of an incident plane wave, and this is in agreement with a multicrystal experiment.

Simulation of section topographs may be now used as a tool by both theoreticians and experimentalists, but as the latter are more interested in traverse topographs which allow one to examine, in one experiment, a large crystal volume, it would be of great interest to simulate these experiments.

Takagi (1969) has shown that the integrated intensity along the exit surface of a crystal may be calculated from the knowledge of the repartition of intensity, along this surface, due to any kind of incident wave on the crystal. It must be noticed that, in the present case, integrated intensity refers to the intensity falling at a given point P on the exit surface of the crystal for a given reflexion.

If we assume, for simplicity, that the entrance surface of the crystal is a plane, the amplitudes of the two Fourier components of the crystal wave and of the incident wave may be written as:

$$D_a(\mathbf{r}_e)\exp(-i2\pi\mathbf{K}\cdot\mathbf{r}_e)=D_0(\mathbf{r}_e)\exp(-i2\pi\mathbf{k}_0\cdot\mathbf{r}_e)$$
$$0=D_{\mathbf{h}}(\mathbf{r}_e)\exp(-i2\pi\mathbf{k}_{\mathbf{h}}\cdot\mathbf{r}_e) \quad (1)$$

where $\mathbf{K}$ is the wave vector of the incident wave of amplitude $D_a(\mathbf{r}_e)$; $\mathbf{r}_e$ indicates a point on the entrance surface of the crystal (Fig. 1). If we introduce a coordinate ξ along this surface, (1) may be written as:

$$D_0(\xi)=D_a(\xi)\exp(-i2\pi T\xi) \quad (2)$$

where $T=(\mathbf{K}-\mathbf{k}_0)\cdot\mathbf{r}_e$.

The integrated intensity at a point P, in the crystal, is obtained by the integration of $D_{\mathbf{h}}(P)D^*_{\mathbf{h}}(P)$.

The amplitude of the reflected wave $D_{\mathbf{h}}(P)$ depends on the boundary conditions expressed in (1), which are characterized by the phase factor T.

The integrated intensity is given by:

$$I_{\mathbf{h}}(P)=\int_{-\infty}^{+\infty}\mathrm{d}T\int\int_{BA}U_{\mathbf{h}}(P,\xi)D_a(\xi)U^*_{\mathbf{h}}(P,\xi')D^*_a(\xi')\times K\gamma_0\exp[-i2\pi T(\xi-\xi')]\mathrm{d}\xi\mathrm{d}\xi', \quad (3)$$

$\gamma_0=\cos(\mathbf{n},\mathbf{s}_0)$ (Fig. 1).

$U_{\mathbf{h}}(P,\xi)$ is the amplitude of a reflected wave corresponding to an incident wave which would be a point source located at the coordinate ξ on the entrance surface.

We may change the order of integration, and as:

$$\int_{-\infty}^{+\infty}\exp[-i2\pi T(\xi-\xi')]\mathrm{d}T=\delta(\xi-\xi')$$

the integral (3) may be written as

$$I_{\mathbf{h}}(P)=\int_{BA}|U_{\mathbf{h}}(P,\xi)|^2|D_a(\xi)|^2K\gamma_0\mathrm{d}\xi. \quad (4)$$

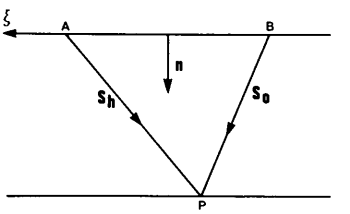

Fig. 1. Notations used in the Takagi–Taupin equations.

In (3) and (4) we have neglected a constant factor which should appear in front of the integrals.

The integral (4) means that, at the point P on the exit surface, the integrated intensity I_h is given by the superposition of the intensities of elementary diffracted waves along the entrance surface.

This is a very important point because it means that the intensity, in a traverse topograph, is determined by the total intensity arriving at each point P on the exit surface and is completely independent of the intensity distribution or the shape of the wave front incident on the crystal.

If we consider the two practical cases where the incident wave is a plane wave or a spherical wave,

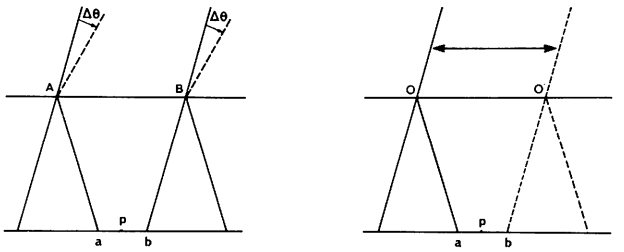

Fig. 2. The two ways of calculating the intensity along ab, on a traverse topograph. (a) Addition of incident plane waves with departures $\Delta\theta$ from the Bragg angle. (b) Simulation of the real experiment with a translation OO' of the source.

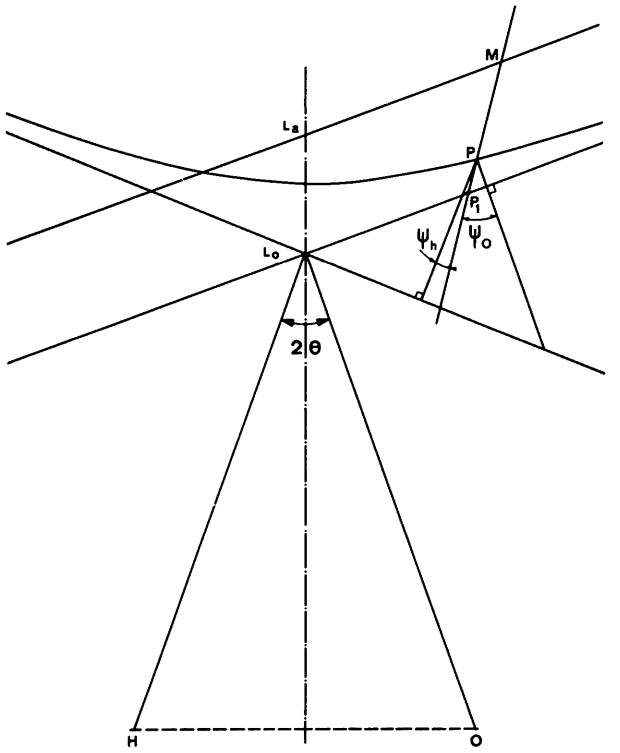

Fig. 3. Conditions of continuity along the entrance surface. For simplicity, branch 1 only of the hyperbola has been drawn.

Authier & Simon (1968) have shown that the corresponding amplitudes of the waves, inside the crystal, are linked by a Fourier transform. The reciprocal variables of this transformation are the position of the point P, on the exit surface, where the intensity I_h is calculated in the case of an incident spherical wave and the phase T in the case of an incident plane wave. We will show that this phase is related to the departure from the Bragg angle of the incident wave.

This means that the integral (4) results from the application of Parseval's theorem and that the integrated intensity may be calculated in two different ways with both reciprocal variables used as parameters of the integration: (a) by adding the intensities due to incident plane waves with different phases, *i.e.* with variable departures from the Bragg angle (Fig. 2a). (b) by simulating the real procedure of a traverse topograph, *i.e.* to move the position of a spherical source on the entrance surface and to add the intensities of each calculation (Fig. 2b).

From the theoretical point of view the methods are equivalent, but for a simulation we must use that which corresponds to the fastest calculation; since the integrals must be replaced by numerical algorithms in the computation we must discuss the approximations which will be introduced. Then we will be able to choose the best method to calculate the contrast of a defect in a traverse topograph.

The last part of this paper presents the result of the calculation by both methods and we shall explain why it is not possible, in reality, to simulate traverse topographs with good accuracy.

I. Numerical methods of integrating the Takagi–Taupin equations

Let us recall the well-known equations (Takagi, 1962; Taupin, 1964) which give the amplitudes of both refracted and reflected waves D_0 and D_h

$$\frac{\partial}{\partial s_0} D_0(\mathbf{r}) = -i\pi K \chi_{\bar{h}} D_h(\mathbf{r})$$

$$\frac{\partial}{\partial s_h} D_h(\mathbf{r}) = -i\pi K \chi_h D_0(\mathbf{r}) + 2i\pi\{K\beta_h - \frac{\partial}{\partial s_h}[\mathbf{h}\,.\,\mathbf{u}(\mathbf{r})]\} D_h(\mathbf{r}) \qquad (5)$$

where χ_h and $\chi_{\bar{h}}$ are the Fourier coefficients of the electric susceptibility. As is usual in simulation routines, we will neglect polarization effects, thus $C=1$. $\mathbf{u}(\mathbf{r})$ is the local deformation of the crystal at the point $\mathbf{r}$; $\mathbf{h}$ is the reciprocal vector of the reflexion. $\beta_h = (|\mathbf{k}_h| - |\mathbf{k}_0|)/|K|$; its value will be chosen to simplify the relations of continuity between the vacuum and the entrance surface of the crystal, which correspond to (1). The extremities of both vectors $\mathbf{k}_h$ and $\mathbf{k}_0$ are matched through the value of β_h and its choice must be made so that the amplitudes $D_0(\mathbf{r})$ and $D_h(\mathbf{r})$ are

slowly varying functions of the position inside the crystal. If we choose:

$$|\mathbf{k}_0| = k = K(1+\chi_0/2)\,,$$

where k is the mean wave number in the crystal, any slight variation of $\mathbf{k}_0$ may be written in the expression of the amplitudes. All explanations may be found in Takagi (1975*a*). The extremity of $\mathbf{k}_0$ will thus lie on a sphere of radius $K(1+\chi_0/2)$ which is, in a plane of incidence, the asymptote to the dispersion hyperbola. In the integration routine we will choose this extremity at the point P_1 (Fig. 3) which is the intersection of the asymptote with the normal to the entrance surface drawn from the characteristic point M in the vacuum.

Let us consider now the phase factor which appears in (1); its value will be equal to zero and this will simplify in the integration routine the continuity equations which may now be written as

$$D_0(\xi) = D_a(\xi)\,.$$

A simple calculation shows that:

$$\beta_{\mathbf{h}} = -\eta\sqrt{(\chi_{\mathbf{h}}\chi_{\bar{\mathbf{h}}})}/(\gamma_{\mathbf{h}}/\gamma_0) \qquad (7)$$

where η is the usual deviation parameter which gives the value of the departure from the Bragg angle;

$$\gamma_0 = \cos(\mathbf{n}, \mathbf{s}_0)$$
$$\gamma_{\mathbf{h}} = \cos(\mathbf{n}, \mathbf{s}_{\mathbf{h}}) \quad \text{(Fig. 1)}\,.$$

We will now examine the approximations which appear in the numerical method of integration of (5).

We will only recall the principles which have been explained in other papers (Authier, Malgrange, Tournarie, 1968; Epelboin, 1975*a*, *b*).

The crystal is divided in elementary slabs (Fig. 4) and the integration is performed along a network parallel to the refracted and reflected directions $\mathbf{s}_0$, $\mathbf{s}_{\mathbf{h}}$. Let p and q be the elementary steps along both directions.

$$p = \gamma_0 \mathrm{ELEM}$$
$$q = \gamma_{\mathbf{h}} \mathrm{ELEM}$$

where ELEM is the thickness of a slab.

Equations (5) may be written:

$$p\frac{\partial}{\partial s_0} D_0 = 2AD_{\mathbf{h}}$$

$$q\frac{\partial}{\partial s_{\mathbf{h}}} D_{\mathbf{h}} = 2BD_0 + 2WD_{\mathbf{h}}$$

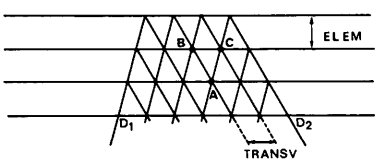

Fig. 4. Principles of the integration of the Takagi–Taupin equations, step by step.

where

$$A = -\tfrac{1}{2}ip\pi K\chi_{\bar{\mathbf{h}}}$$
$$B = -\tfrac{1}{2}iq\pi K\chi_{\mathbf{h}}$$
$$W = i\pi q\left\{K\beta_{\mathbf{h}} - \frac{\partial}{\partial s_{\mathbf{h}}}[\mathbf{h}\,.\,\mathbf{u}(\mathbf{r})]\right\}. \qquad (8)$$

Only W is a function of the position inside the crystal.

II. Approximations of the method of integration

II.1. *First approximation*: '*half-step derivative*'

We use the so-called method of the 'half-step derivative' to evaluate the values of $\partial D_0/\partial s_0$ and $\partial D_{\mathbf{h}}/\partial s_{\mathbf{h}}$. If we write the following developments of a function $f(x)$.

$$f(x) = f(x+p/2) - P/2\frac{\partial}{\partial x}f(x+p/2) + p^2/8\frac{\partial^2}{\partial x^2}f(x+p/2) - p^3/48\frac{\partial^3}{\partial x^3}f(x+p/2)$$

$$f(x+p) = f(x+p/2) + P/2\frac{\partial}{\partial x}f(x+p/2) + p^2/8\frac{\partial^2}{\partial x^2}f(x+p/2) + p^3/48\frac{\partial^3}{\partial x^3}f(x+p/2)$$

we may write that

$$p\frac{\partial}{\partial x}f(x+p/2) = f(x+p) - f(x)$$

with an error of third order only: less than

$$p^3/24\frac{\partial^3}{\partial x^3}f(x+p/2)\,.$$

The Takagi–Taupin equations may thus be written in the form:

$$D_0(s_0, s_{\mathbf{h}}) - D_0(s_0 - p, s_{\mathbf{h}}) = 2AD_{\mathbf{h}}(s_0 - p/2, s_{\mathbf{h}})$$
$$D_{\mathbf{h}}(s_0, s_{\mathbf{h}}) - D_{\mathbf{h}}(s_0, s_{\mathbf{h}} - q) = 2BD_0(s_0, s_{\mathbf{h}} - q/2) + 2W(s_0, s_{\mathbf{h}} - q/2)D_{\mathbf{h}}(s_0, s_{\mathbf{h}} - q/2)\,. \qquad (9)$$

II.2. *Second approximation*

As D_0 and $D_{\mathbf{h}}$ vary slowly with the position inside the crystal, we may write them at position $s_0 - p/2$, $s_{\mathbf{h}}$ or s_0, $s_{\mathbf{h}} - q/2$ with the following approximation:

$$2f(x+p/2) \simeq f(x) + f(x+p/2)\,.$$

Now the error will be less than

$$p^2/4\frac{\partial^2}{\partial x^2}f(x+p/2)$$

which is of second order only. So, we may write the following system which will be used in the integration routine:

$$\begin{bmatrix} D_0(s_0,s_h) \\ \\ D_h(s_0,s_h) \end{bmatrix} = 1/d \begin{bmatrix} C_2AC_2ABAC_1 \\ B\ AB\ B\ C_1 \end{bmatrix} \begin{bmatrix} D_0(s_0-p,s_h) \\ D_h(s_0-p,s_h) \\ D_0(s_0,s_h-q) \\ D_h(s_0,s_h-q) \end{bmatrix} \quad (10)$$

where $d=1-W-AB$, $C_1=1+W$, $C_2=1-W$.

It must be noticed that Taupin (1964, 1967) uses a Runge–Kutta method to integrate the equations. This method is more precise but needs more computer time: we will show that, in a simulation, this accuracy is lost for reasons which will be explained in the following paragraphs.

II.3. *Numerical approximations*

Equations (9) show clearly that the values of the amplitudes D_0 and D_h at a given point A (Fig. 4) depend only on the values of the amplitudes at points B and C. If the thickness of the slab, ELEM, is small enough to take into account the slow variations of the amplitudes, we shall finally obtain the values of the intensity on the exit surface through the iteration which is given in equations (10). But the numerical values of the variables may be written in the computer with a limited number of digits, and as the numerical approximation in each elementary operation of the routine is of the order of the last bit, at least, the error will rapidly increase with the number of elementary slabs. For example, suppose the crystal is divided into 400 elementary slabs; to use a 32-bit word (which is the case with IBM computers) means that the final value of the intensity will be known with an error on the fourth or fifth digit. This is not very important in the simulation of a section topograph.

Of course all the different approximations decrease the accuracy of the calculation, but we must remember that the worst part of the simulation is the final stage: the representation of a photographic picture by means of a lineprinter; the error made there is much larger than any due to the approximations we have already discussed. In any case, it does not seem that the approximations will strongly affect a simulation. It is of more importance in the case of a traverse topograph: we shall have to add the calculated values of the intensities from different incident waves arriving at the same point on the exit surface.

Thus, the numerical approximation from the computation will also be proportional to the number of added waves and may become of great importance. Of course, we may increase the precision of the calculation by using longer words in the computer but this means more core memory and a longer computing time. On the other hand, we may save time by using a step of integration which varies with the importance of the local deformation inside the crystal. This has been done by Taupin (1967) and by Takagi *et al.* (1974) for the case of a crystal containing a dislocation. The interest of such a method depends upon the computer and has been discussed in a preceding paper (Epelboin, 1975*b*).

But we will now see that the main limitation in the simulation of a traverse topograph comes from the errors which appear in the boundary conditions.

III. Boundary conditions

As has already been explained, we have two practical choices for the calculation of the integrated intensity in the case of a traverse topograph: to add the intensities either for an incident plane wave or for an incident spherical wave; we will therefore examine the boundary conditions in both cases.

III.1. *Spherical incident wave*

A spherical incident wave may be simulated, to a good approximation, by the light from one point source on the entrance surface of the crystal. The value of β_h has no importance and may be taken equal to zero. This is a good approximation for an incident spherical wave, as has been explained by Kato (1976): if we calculate the intensity distribution on the exit surface of the crystal, it may be shown that the result is the well-known Bessel function (Kato, 1961) when the elementary step of integration is decreased to zero. But troubles stem from this good approximation itself: the Bessel function J_0 varies rapidly near the $\mathbf{s}_0$ and $\mathbf{s}_h$ directions.

If we plot the repartition of intensity in a perfect crystal along a line parallel to the entrance surface (Fig. 5) the greatest part of the intensity appears near the edges of the Borrmann triangle, before the first zero of the J_0 Bessel function. Thus, if the vertical step of integration ELEM is not small enough, the corresponding horizontal step TRANSV (Fig. 4) may be too large to take into account the rapid variations of J_0. Table 1, due to Takagi (1975*b*) gives the value H (Fig. 5) of the first zero of $J_0(H)$ as a function of the thickness Z of the crystal.

For example, if we simulate a section topograph in a 800 μm thick silicon crystal, using the 220 reflexion with Mo $K\alpha$ radiation (Epelboin, 1974), $Z=20{\cdot}3\,\Lambda/\pi$ where Λ is the extinction distance; the horizontal step

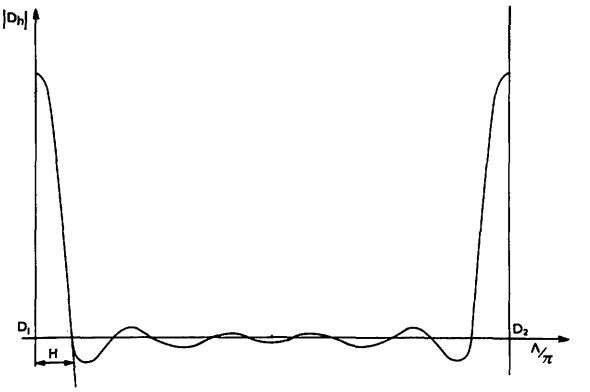

Fig. 5. Amplitude of the reflected wave in a perfect crystal, with low absorption, along a line parallel to the surface.

Table 1. *First zero of the J_0 Bessel function as a function of Z, thickness of the crystal, in units of Λ/π*

Z	10	20	50
H	0·15	0·07	0·03

is TRANSV = 0·066 Λ/π. This means that in the simulation a great part of the intensity will be missing along the $\mathbf{s}_0$ direction, because the horizontal step is too large. This will be important only for the kinematical image of a dislocation when this defect crosses the refracted beam, because the greatest part of the intensity lies along the $\mathbf{s}_0$ direction inside the crystal but will only slightly affect the other parts of the image. This explains why the kinematical image is never good in a simulation.

Consider now the case of a traverse topograph: this error will certainly be more important than all the approximations which have been made in the integration. It is well known (Authier, 1961) that in low-absorbing crystals the image of a defect in a traverse topograph is mainly due to the kinematical image; so we may assume before any calculation that the values of the integrated intensity obtained by adding spherical incident waves will certainly be lower than in the real experiment.

III.2. *Incident plane wave*

A good approximation for the simulation of an incident plane wave, is the light from many point sources on the entrance surface of the crystal (Authier, Malgrange & Tournarie, 1968).

In this case the value of $\beta_{\mathbf{h}}$ will characterize the departure from the Bragg angle of the incident wave [equation (7)]. We must be careful about the horizontal step of integration, TRANSV. Table 2 gives the variation of the phase of the incident plane wave, given in (2), as a function of η along the entrance surface (Fig. 1).

Table 2. *Variation of the phase of an incident plane wave along the entrance surface in units of 2π*

ξ	0·9	2·7	9	89·8 Λ/π
η				
1	0·77	2·31	7·71	77·14
20	15·42	46·28	154·29	1542·89

For example, let us consider the same experimental conditions as in the discussion about the incident spherical wave; to simulate a plane wave with a limited width of ~ 30 μm corresponds to about 40 points of light along the entrance surface. Expressed in terms of Λ this width is equal to $2{\cdot}7\,\Lambda/\pi$. For $\eta = 1$ this means that the phase varies along the wave front on the entrance surface from zero to $2{\cdot}31 \times 2\pi$. 40 points are enough to take into account the oscillations of this phase, but will certainly be wrong for high values of η: in this case the phase varies from zero to $46{\cdot}28 \times 2\pi$ and we should decrease the integration step to match the boundary conditions along the entrance surface correctly. But, as we have already explained in § I, this problem does not appear in our routine: the extremities of the wave vectors $\mathbf{k}_0$ and $\mathbf{k}_{\mathbf{h}}$ have been chosen on the normal to the entrance surface of the crystal, at point P_1 (Fig. 1) and the phase of the incident wave, given in (2), is thus always equal to zero along the entrance surface. This does not mean that the length of the integration step has no importance. To evaluate its influence let us write the conservation of energy in a perfect non-absorbing crystal:

$$\mathscr{I} = \sum \gamma_0 D_0 D_0^* + \sum \gamma_{\mathbf{h}} D_{\mathbf{h}} D_{\mathbf{h}}^* .$$

The summation must be done at each point of the network of integration along a line D_1D_2 (Fig. 4) parallel to the slab of thickness ELEM. It may be shown (Authier, Malgrange & Tournarie, 1968) that the total energy will be:

$$\mathscr{I} = 1 + 2\alpha |ABW^2|$$

where α is the energy flow in the reflected direction and $1-\alpha$ the energy flow in the refracted direction. The intensity of the incident wave is normalized and equal to unity. In the case of a symmetric reflexion, and in a perfect crystal:

$$W = i\pi q K \beta_{\mathbf{h}} ,$$

thus

$$|W| = \pi(\mathrm{ELEM}/\cos\theta)K|/(\chi_{\mathbf{h}}\chi_{\bar{\mathbf{h}}})|\eta| .$$

Assuming that the energy is of the same order in both diffracted and reflected directions, the error is of the order of $|ABW^2|$. Thus, for the same simulation as before, the error is of the order of $10^{-5}\,\eta^2$. This means that the accuracy of the simulation will decrease very rapidly when η increases.

By a good choice of the extremities of the wave vectors $\mathbf{k}_0$ and $\mathbf{k}_{\mathbf{h}}$ we have overcome the problem of the sampling of the phase of a plane wave along the entrance surface of the crystal, but a difficulty then arises in the conservation of the energy flow. This means that the simulation of a traverse topograph by addition of the intensities of incident plane waves will suffer an error directly proportional to the number of added waves. Moreover, the errors will become more important as the departure from the Bragg angle becomes more important and thus the convergence of the integral (3) may be lost, or we may obtain oscillating solutions for the integrated intensity along the exit surface of the crystal.

IV. Results of the simulation

We have calculated the contrast of a dislocation in a silicon crystal 226 μm thick. The dislocation lies parallel to the surface of the crystal; its Burgers vector is $\frac{1}{2}[10\bar{1}]$ and its depth, inside the crystal, is 200 μm. The reflexion vector is 220 with Mo $K\alpha$ radiation. It is a symmetric reflexion since the normal to the en-

trance surface is [111] (Fig. 6). The linear photoelectric absorption is $\mu = 1{\cdot}42\ \text{mm}^{-1}$. The integration was performed through 113 elementary slabs of thickness ELEM = 2 μm.

The contrast of the dislocation on a traverse topograph has been calculated by adding the intensities due to incident plane or spherical waves. Both methods should be equivalent but the aim was to obtain a good convergence of integral (3) by addition of a few plane waves only and thus to obtain the contrast of the defect with an acceptable accuracy in a reasonable time. We will explain that the reality is quite different!

IV.1. *Integration by addition of incident plane waves*

Each added plane wave was 580 μm wide on the entrance surface *AB* (Fig. 2*a*) which corresponds to a usable width *ab* of 496 μm on the exit surface. We have added up to 121 different plane waves with departures from the Bragg angle ranging from $-0{\cdot}6 \times 10^{-4}$ to $0{\cdot}6 \times 10^{-4}$ rad with a regular angular step of 10^{-6} rad. The corresponding limits in term of η are $\eta \simeq \pm 11$.

The first question is to know how large the limits of integration should be in order to obtain good accuracy in the calculation of integral (3). Let us assume for simplicity that in a perfect crystal (taking an average over the *Pendellösung* oscillations) the intensity of the reflected beam is proportional to $1/(1+\eta^2)$ (Authier, 1961). Thus the integrated intensity I_h is proportional to the integral:

$$I_h \sim \int_{-\infty}^{+\infty} [1/(1+\eta^2)]\mathrm{d}\eta = \pi .$$

The accuracy of the calculated integral may thus be estimated to be of the order of:

$$\frac{1}{\pi}\int_{\eta_{\min}}^{\eta_{\max}} [1/(1+\eta^2)]\mathrm{d}\eta$$

where $\eta_{\min}$ and $\eta_{\max}$ are the limiting values of the departure from the Bragg angle. Table 3 gives the accuracy of the integration for different values of the limits of integration; in each case $\eta_{\min} = -\eta_{\max}$. It seems that the accuracy is good enough when $|\eta| = 11$ and we did not try to take greater values for the limits of the integral.

The second problem is to choose the magnitude of the angular step of integration, *i.e.* the variation of the departure from the Bragg angle from one incident plane wave to the next. On one hand, it is advisable to choose the smallest angular step of integration, but this means that for given limits of integration a greater number of waves should be added and that the accuracy of the integral will rapidly decrease, as has been explained in § II.3; we must also take into account the time of computation which is directly proportional to the number of added waves. On the other hand, too large an angular step means a loss of accuracy in the integral.

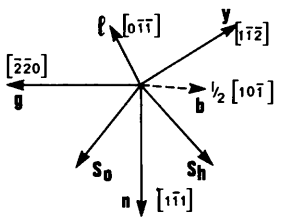

Fig. 6. Geometry of the dislocation in the simulation. l indicates the direction of the line.

Table 3. *Estimation of the accuracy of integral* (3) *with limits equal to* $\pm|\eta|$

$\lvert\eta\rvert$	2	5	9	11	15	20	30
Accuracy %	29·5	12·6	7	5·7	4·2	3·2	2·1

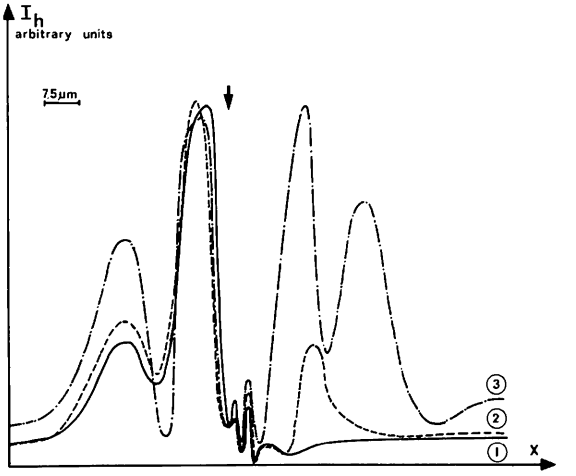

Fig. 7. Integrated intensity along the exit surface of the crystal from *a* to *b* (Fig. 2*a*). Limits of integration $\Delta\theta = \pm 0{\cdot}45 \times 10^{-4}$ rad. (1) Angular step of integration $\delta(\Delta\theta) = 10^{-6}$ rad. (2) Step equal to 2×10^{-6} rad except between $-0{\cdot}3 \times 10^{-4}$ rad and $0{\cdot}3 \times 10^{-4}$ rad where it is equal to 10^{-6} rad. (3) Same as curve 2 except between $-0{\cdot}15 \times 10^{-4}$ and $0{\cdot}15 \times 10^{-4}$ rad where the step is equal to 10^{-6} rad. The arrow denotes the projection of the dislocation on the exit surface of the crystal.

Let us first check the value of the angular step of integration. Fig. 7 represents the results of the computation for $\Delta\theta$ varying from $-0{\cdot}45 \times 10^{-4}$ rad to $0{\cdot}45 \times 10^{-4}$ rad. ($\eta \simeq \pm 8{\cdot}2$). Curve 1 corresponds to the addition of 91 waves with an angular step of 10^{-6} rad. Curves 2 and 3 correspond to the same calculation but the step has been increased for the greater values of the departure from the Bragg angle. In both curves the angular step remains the same as before for the low values of departure from the Bragg angle, but has been doubled for the highest values.

The three curves of this figure are quite different. Clearly, the calculation is not stable and we must choose as small as possible an integration step. This is confirmed in Fig. 8, where the limits of integration are larger ($\Delta\theta = \mp 0{\cdot}6 \times 10^{-4}$ rad and where we have increased the step of integration for the smaller values

of this step. We have also tried to decrease the angular step of integration from 10^{-6} rad to $0{\cdot}5 \times 10^{-6}$ rad. This is presented in Fig. 9. The first peak on the left is an artefact due to the small values of the limits of the integral but the two curves are very similar. This suggests that an angular step of 10^{-6} rad is small enough to obtain a good convergence.

Let us now check the importance of the limits of integration. Curves 1 in Figs. 7 and 8 are quite different: a peak on the right of the curve appears when the limits of the integral are increased; this may be explained as follows. The kinematical image of a defect is due to X-rays which propagate along the refracted reflexion and which are quite far from the exact Bragg position; the same contribution appears from incident waves with a large departure from the Bragg angle. This peak on the right is thus due to the kinematical image and its height will increase when the limits of integration are larger: it is not yet visible on curve 1 of Fig. 7 but appears clearly on curve 1 of Fig. 8. This is more apparent on the three curves of Fig. 10 where the step of integration is fixed and where the limits of the integral are enlarged from one curve to another.

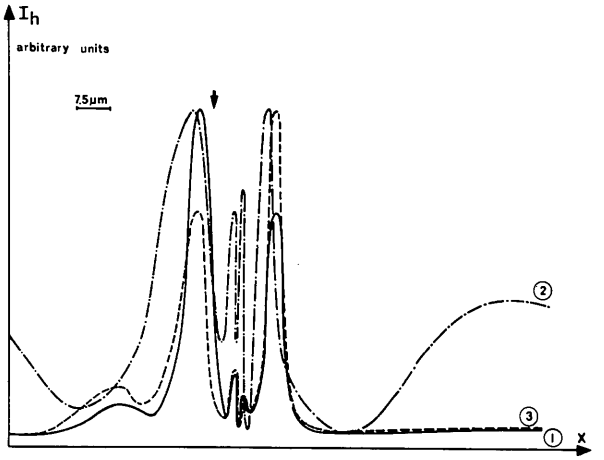

Fig. 8. Integrated intensity as in Fig. 7. Limits of integration $\mp 0{\cdot}6 \times 10^{-4}$ rad. (1) Angular step 10^{-6} rad. (2) Same angular step except between $\mp 0{\cdot}15 \times 10^{-4}$ rad, step equal to 2×10^{-6} rad. (3) Angular step equal to 2×10^{-6} rad between $\mp 0{\cdot}45 \times 10^{-4}$ rad.

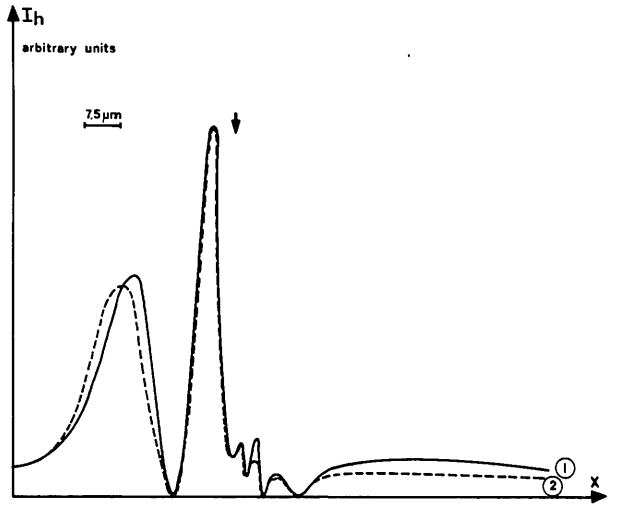

Fig. 9. Integrated intensity as in Fig. 7. Limits of integration $\mp 0{\cdot}15 \times 10^{-4}$ rad. (1) Angular step 10^{-6} rad. (2) Angular step $0{\cdot}5 \times 10^{-6}$ rad.

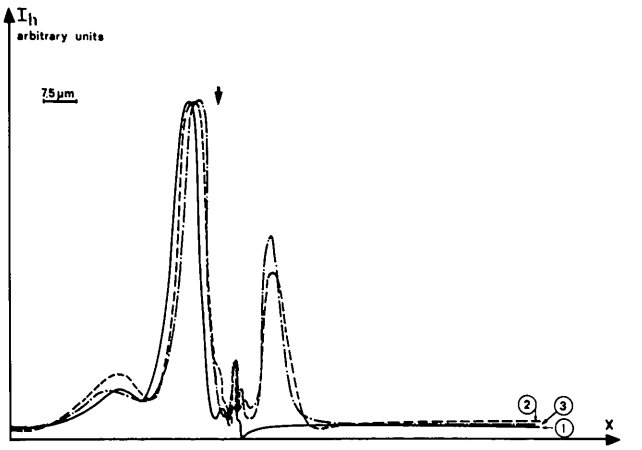

Fig. 10. Integrated intensity as in Fig. 7. Step of integration 10^{-6} rad. Limits of the integral: (1) $\pm 0{\cdot}4 \times 10^{-4}$ rad, (2) $\pm 0{\cdot}5 \times 10^{-4}$ rad, (3) $\pm 0{\cdot}55 \times 10^{-4}$ rad.

Another characteristic phenomenon is the disappearance of a peak on the left of the curves when the limits of the integral are enlarged: to add more and more waves decreases the height of this peak. This may be understood by the simulation of the paths of the reflected wave fields inside the crystal. Fig. 11(*b*) shows the repartition of the intensity in a plane of incidence for an edge dislocation perpendicular to this plane, when the incident wave is a plane wave. The departure from the Bragg angle is null, thus $\eta = 0$. We notice the presence of two important directions of propagation of the wave fields below the defect. The beam on the left corresponds to the peak on the left of the curves in the limiting case when we add only one wave.

Consider now Fig. 11(*a*) where the incident wave is a spherical wave. We do not notice any direction of propagation on the left side of the picture, below the defect. This corresponds to the limiting case when we add an infinite number of plane waves. The beam on the left side of the figure disappears when passing from the plane wave to the spherical wave. This suggests that the peak which disappears in the curves presented in this paper when the limits of the integral are increased, corresponds to wave fields with a small departure from the Bragg angle and should disappear when the limits of the integral are large enough, as in the case of the Fig. 8, curve 1.

We may conclude that (1) the integration is very sensitive to the value of the limits and that we must take them as large as possible. This may be explained by the appearance of the kinematical image of the defect and by a greater accuracy of the calculation (see Table 3). But the sampling of the sources along the entrance surface is very critical for large departures from the Bragg angle, as explained in § III.2, and the calculation may be erroneous for large departures. Thus we must optimize both conditions. (2) The integration step must be as small as possible and it would be interesting to decrease it more than we have done. But then the approximations of the numerical calculation may not longer be justifiable (see § II.3). A simple calculation shows that in the calculated profile of Fig. 8, curve 1 the error is of the order of the third digit, using simple precision with a 32-bit word. This difficulty may be overridden but requires important changes in the routine, the use of a large core memory and more computer time. It does not present any interest as will be explained in § V.

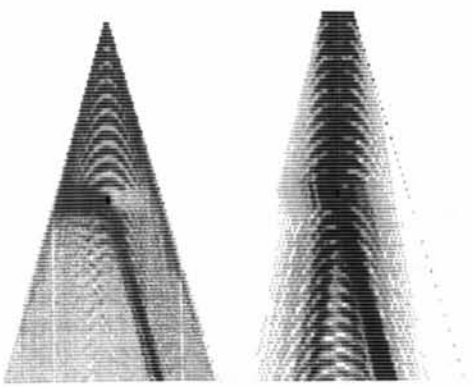

Fig. 11. Simulation of the paths of the reflected wave fields for an edge dislocation, in a silicon crystal 800 μm thick. Reflexion 220 Mo $K\alpha$ (after Epelboin, 1975*a*). (*a*) Incident spherical wave. (*b*) Incident plane wave with $\eta = 0$.

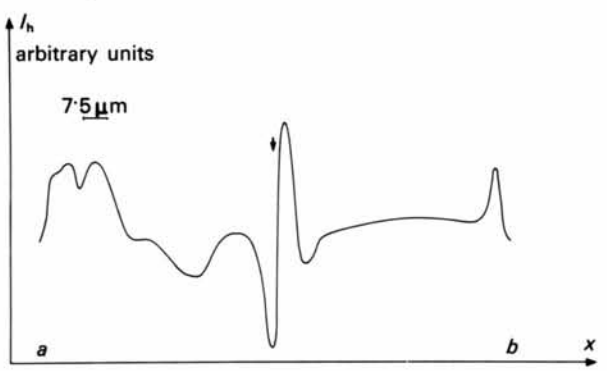

Fig. 12. Integrated intensity along the exit surface of the crystal. Same defect as before, but simulation of the real experiment by addition of incident spherical waves.

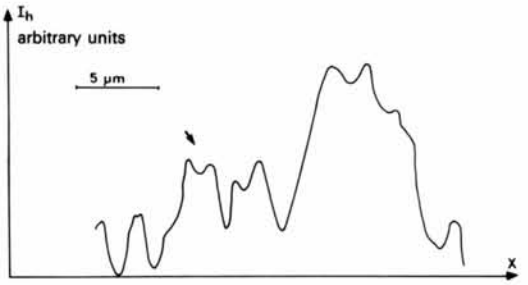

Fig. 13. Densitometric measurement of the contrast of the defect simulated in this paper (due to Dr B. K. Tanner).

IV.1. *Integration by addition of incident spherical waves*

The calculation of the contrast of a traverse topograph by addition of incident spherical waves corresponds to a direct simulation of the real experiment: we have translated the point source along the entrance surface of the crystal as described in Fig. 2(*b*). The number of a spatial steps has been chosen in agreement with the network of integration of the Takagi–Taupin equations: it is equal to the horizontal step of this network TRANSV (Fig. 4).

In order to obtain the integrated intensity along a length *ab* (Fig. 2*b*) equal to 150 μm, we have added 300 different waves. The result (Fig. 12) is quite different from the corresponding result obtained by addition of incident plane waves (Fig. 8, curve 1). (1) The left peak of Fig. 8, curve 1 is decreased and its height is of the order of the mean intensity along the traverse topograph in Fig. 12. (2) The right peak is not at the same position in both figures with respect to the projection of the defect on the exit surface of the crystal. We must also notice the presence of two important peaks on both wings of the curve of Fig. 12.

We have compared both theoretical profiles with an experimental profile (Fig. 13). The large peak corresponds to the image of the defect; the second, on the left, indicated by an arrow, is due to the noise of the plate. The profile calculated by addition of incident spherical waves is more in agreement with experiment; the width of the main peak is larger in the experiment, but this may be explained by the width of the entrance slit of the X-rays, which is of the order of 100 μm. The two peaks on the wings will be explained in the next section.

We must conclude that the correlation between the experiment and the calculation is not very good.

V. Fundamental difficulties in the simulation of traverse topographs

In a perfect crystal the amplitude of the reflected waves at a given point P on the exit surface corresponds to the convolution of the repartition of light sources along the entrance surface of the crystal with the J_0 Bessel function (Balibar, 1969). This function oscillates

very rapidly along the limits of the integral PA and PB (Fig. 1).

Takagi (1975*b*) has explained that the propagation of the wave fields will take place along the directions where the oscillations of the phase of the sources and of the J_0 Bessel function are in greatest agreement. The greatest part of the intensity will thus come from the edges of the triangle PA and PB (Fig. 1) where the oscillations of J_0 are more important (Fig. 5).

Let us now suppose that the incident wave on the entrance surface AB of the crystal is a plane wave. The phase of this wave varies in agreement with (2). In the numerical integration of the Takagi–Taupin equations the error due to a distribution of sources along AB will then be more important when the oscillations of J_0 are noticeable, thus, the main error at point P on the exit surface will come from the values of the amplitude of the incident wave around A and B. In the simulation of the traverse topograph by addition of incident plane waves we will add the errors due to each plane wave, and the total error will be proportional to the number of added waves.

Moreover, as has been explained in § III.2, numerical errors appear when we add plane waves with large departures from the Bragg angle.

It was therefore possible to predict, before any calculation, that the integration of (3) would not be satisfactory and that the simulation of a traverse topograph by a sum of incident plane waves would give a poor result. This has been confirmed by our simulation and our results show that there is no hope of finding an approximate contrast by the addition of only a few plane waves, which was the only interest of such a method.

Consider now the simulation of a traverse topograph by the addition of spherical incident waves. The distribution of sources is limited to one point on the entrance surface AB. The approximations of the integration will be noticeable only when the source lies in regions where the oscillations of J_0 are noticeable, *i.e.* near A and B. The error in the value of the integrated intensity at point P would thus be important only for a small number of added waves, of the order of the error due to an integration performed with a single incident plane wave. It is another way of explaining why a part of the direct image of the defect is missing.

The two peaks on the wings of the curve in Fig. 12 correspond to the limits of the traverse topograph. The simulation is not complete and some of the wave fields are missing; thus the image is wrong and the error due to the oscillations of the Bessel function is more important. A simple drawing shows that these parts correspond to a maximum number of approximations.

VI. Conclusion

We have discussed all the approximations which are made in the numerical integration of the Takagi–Taupin equations. Two different types of errors appear: some are due to the numerical method itself, others are due to the use of a computer. To decrease the order of these approximations means writing more sophisticated routines and also working with computers which possess a maximum word length. As up to now the simulation of a section topograph has required a long computing time, it is not of practical interest to simulate section topographs with greater accuracy; we have shown that the actual precision of a simulation is good enough. In the case of a traverse topograph, it appears clearly that the solution is to simulate the real experiment, *i.e.* to add the repartition of intensity due to incident spherical waves. The calculation by means of incident plane waves comes up against two difficulties: the choice of the limits of integration and the step size of this calculation. We may conclude that the use of plane waves does not present any interest for the simulation of traverse topographs.

To obtain a good simulation of a traverse topograph we must decrease the order of the approximations. In the present work, a complete integration of the Takagi–Taupin equations through the whole crystal, was performed in 1·2 s, with incident spherical waves (on an IBM 370/168 computer); the total calculation of the intensity in the traverse topograph was made in about 6 min. To simulate a traverse topograph whose height is of the order of its width would mean 2 h of computer time! This means that the simulation of a traverse topograph with a greater accuracy than the present would take many hours.

We may therefore conclude that the simulation of traverse topographs by the means of a computer has no actual practical interest. We must find a way other than an integration of the Takagi–Taupin equations along a network parallel to the edges of the Borrmann fan in order to simulate translation topographs.

All the discussion of § § III and V is based on discussions and seminars held by Professor S. Takagi at the laboratory. I am very indebted to him for his kind attention. Thanks are due to Dr B. K. Tanner for providing experimental data and densitometric measurements.

References

AUTHIER, A. (1961). *Bull. Soc. Fr. Minér. Crist.* **84**, 51–103.
AUTHIER, A. & BALIBAR, F. (1967). *Phys. Stat. Sol.* **21**, 413–422.
AUTHIER, A., MALGRANGE, C. & TOURNARIE, M. (1968). *Acta Cryst.* A**24**, 126–136.
AUTHIER, A. & SIMON, D. (1968). *Acta Cryst.* A**24**, 517–526.
BALIBAR, F. (1969). *Acta Cryst.* A**25**, 650–658.
BEDYNSKA, T. (1973). *Phys. Stat. Sol.* (*a*), **18**, 147–154.
CHUKOVSKII, F. N. (1974). *2nd Eur. Crystallogr. Meeting*, Kesthely, Hungary, pp. 61–62.
EPELBOIN, Y. (1974). *J. Appl. Cryst.* **7**, 372–377.

EPELBOIN, Y. (1975*a*). *Acta Cryst.* A**31**, 591–600.
EPELBOIN, Y. (1975*b*). International Summer School, X-ray Dynamical Theory and Topography, Limoges, France, A**15**,
ISHIDA, H., MIYAMOTO, N. & KOHRA, K. (1976). *J. Appl. Cryst.* **9**, 240–241.
KATO, N. (1961). *Acta Cryst.* **14**, 627–636.
KATO, N. (1976). *Acta Cryst.* A**32**, 453–457.
TAKAGI, S. (1962). *Acta Cryst.* **15**, 1131–1132.
TAKAGI, S. (1969). *J. Phys. Soc. Japan*, **26**, 1239–1253.
TAKAGI, S. (1975*a*). International Summer School, X-ray Dynamical Theory and Topography, Limoges, France, A**10**.
TAKAGI, S. (1975*b*). Private communication.
TAKAGI, S., ISHIDA, H., KOMAKI, K. & SAITO, K. (1974). *Int. Crystallogr. Conf.*, Melbourne, pp. 324–325.
TAUPIN, D. (1964). *Bull. Soc. Fr. Minér. Crist.* **87**, 469–511.
TAUPIN, D. (1967). *Acta Cryst.* **23**, 25–34.

Acta Cryst. (1977). A**33**, 767–770

The Transverse Magnetoresistance of Chromium in the Temperature Range 15–80 °C

BY C. I. SYMEONIDES AND C. N. KOUMELIS

Physics Laboratory, University of Athens, Athens 144, *Greece*

(*Received* 2 *February* 1977; *accepted* 11 *March* 1977)

Electrical measurements have been carried out on a 4*N*5 Cr single crystal in multi-**Q** and single-**Q** domains. It was found that the Néel temperature depends neither on the direction of current, nor on the existence of a magnetic field. In the multi-**Q** domains, the transverse magnetoresistance G changes according to $G = AH^n$. The magnetoresistance decreases with increasing temperature showing an anomaly at 40 °C. For the single-**Q** domain specimen, measurements with $\mathbf{H} \perp \mathbf{Q}$ showed in the antiferromagnetic state the existence of saturation in the curve $G = G(\mathbf{H})$. In the paramagnetic state, the transverse magnetoresistance is an increasing function of the magnetic field. Measurements with $\mathbf{H} \| \mathbf{Q}$ showed that G increases according to $G = AH^n$, and this is ascribed to the existence of open orbits along the direction of polarization.

Introduction

Chromium is an antiferromagnetic material at room temperature, becoming paramagnetic at a somewhat higher temperature. The transition is known as the Néel point and has been found in the region between 35 and 43·5 °C (Corliss, Hastings & Weiss, 1959; Marcinkowski & Lipsit, 1961; Koumelis, 1973).

Cr has kept the interest of many investigators because of the anomalous properties near the Néel temperature, *e.g.* the specific heat, elastic constants, Debye temperature. Of special interest are the anomalies of the electrical properties.

Marcinkowski & Lipsit (1961) measured the resistivity of polycrystalline Cr for various temperatures and found a minimum at 35 ± 2 °C. Arajs & Dunmyre (1965) found this minimum at 40 °C, while Sabine & Svenson (1968) found it at 37 °C. Muïr & Störm-Olsen (1971) measured the resistance of single-**Q** and multi-**Q** Cr *versus* temperature; all their curves showed a minimum at 39 °C, and a common linear part above it. Bastow & Street (1964) measured the temperature dependence of the magnetoresistance for an annealed specimen and found two linear parts that intersected at 38 °C.

Arco, Marcus & Reed (1968) found at 4·2 °K, that a single-$\mathbf{Q} \| [100]$ specimen with the current perpendicular to **Q**, showed a twofold symmetry of the magnetoresistance when the field was rotated around the direction of the current. For single-$\mathbf{Q} \| [001]$ and $i \| \mathbf{Q}$, the magnetoresistance showed a fourfold symmetry upon rotation of the field around the direction of current.

In the present work, the resistance of multi-**Q** and single-**Q** Cr was measured *versus* temperature for a variety of directions of current and magnetic field.

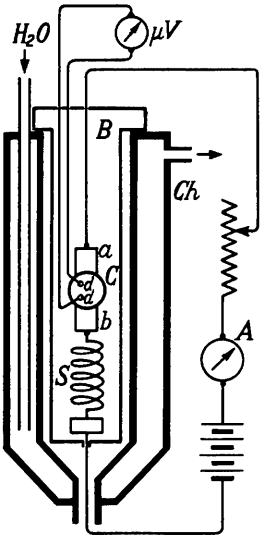

Fig. 1. The heating chamber with the crystal and the electric contacts.